NAVIER-STOKES-BASED DIRECT NUMERICAL AEROELASTIC SIMULATION

G. Britten, J. Ballmann
Mechanics Department, RWTH Aachen University of Technology, Germany

Keywords: *aeroelasticity, CAS, numerical simulation, fluid-structure interaction, elastic wing*

Abstract

This work describes a computational method for the treatment of solid fluid interaction (SOFIA) for the assessment of the aerodynamic performance of large span elastic wings by direct numerical aeroelastic simulation. The fluid flow is modeled by the Euler or by the Reynolds-averaged Navier-Stokes equations. The elastic wing is modeled by a reduced structural model, in this case a generalized Timoshenko-like beam structure. Numerical results including detailed comparison to measured data are shown for a rectangular elastic wing specimen built within the framework of the Collaborative Research Centre SFB401 "Modulation of Flow and Fluid-Structure Interaction at Airplane Wings" of the RWTH Aachen University of Technology.

1 Introduction

The aerodynamic loads acting on the wings of a high capacity aircraft with e.g. a wing span of up to 80m may cause large displacements of the wing's sections. Therefore, the static and dynamic interaction between structural loads and air loads becomes more important than in the case of air planes presently being in service. New design tools which take into account the full nonlinear fluid-structure interaction may even for the first drafts with reduced structural models help to avoid dispensable loops in the design process and thus to meet economic constraints for a faster and cheaper design and construction. One of these tools is the direct numerical aeroelastic simulation, in which the calculation of the flow field and the structural deformation is performed fully coupled and consistent in time. The aerodynamic part of the numerical method SOFIA presented in this paper consists of either an implicit Euler code or a Navier-Stokes code. We use a finite-element-based solver for a multi-axial Timoshenko beam model do discretize the elastic wing structure.

SOFIA is being progressively developed, validated and used in the Collaborative Research Centre SFB401 *"Modulation of Flow and Fluid-Structure Interaction at Airplane Wings"* at RWTH in a mutual exchange with experimental aeroelasticity projects. On one hand it is used to determine loads and appropriate pressure gauge positions. On the other hand the aeroelastic experiments help to validate the code. This paper focuses on the comparison of numerical and experimental results for static aeroelastic equilibrium configurations of a rectangular elastic wing at low wind speeds.

2 Physical Model

2.1 Non-Stationary Flow in a Moving Grid

Two different codes for the calculation of the flow field have been implemented in SOFIA, one solving the Euler equations for unsteady compressible fluid flow, the other integrating the Navier-Stokes equations taking into account additionally viscosity and heat transfer in the fluid.

The governing flow equations are solved by finite volume techniques with control volumina

dependent on time in order to describe consistently the fluid flow and the motion of the wing's surface. Thereby the nodes on the wing's surface are taken as material points of the wing throughout the motion of the structure, whereas the nodes at the outer boundary, which is the boundary of the computational domain, remain fixed in a rigid body fixed coordinate system. Thus, the grid is deforming with time and the nodes of the finite volumes within the flow field are moved such that a grid fitting the body's surface is ensured. The three-dimensional Reynolds-averaged Navier-Stokes equations which are implemented in the FLOWer code read in integral form

$$\frac{\partial}{\partial t}\int\limits_{V(t)} \mathbf{U}dV + \int\limits_{\partial V(t)} \mathbf{F}\mathbf{n}dS + \int\limits_{V(t)} \mathbf{G}dV = 0\,, \quad (1)$$

where $\mathbf{U} = (\rho, \rho u, \rho v, \rho w, \rho e)^T$ is the algebraic vector of conserved quantities: density, Cartesian components of momentum and total specific energy density. Contributions due to the rigid body motion of the grid, which may be rotation with the angular velocity vector $\omega = (\omega_x, \omega_y, \omega_z)^T$, are contained in the source term $\mathbf{G}$ (see [5]). $\mathbf{F} = \mathbf{F}^c + \mathbf{F}^d$ represents the flux function with its parts $\mathbf{F}^c$ designating the convective and in isentropic flows conservative terms and $\mathbf{F}^d$ denoting the diffusive part,

$$\mathbf{F^c} = \begin{bmatrix} \rho(\mathbf{v}-\mathbf{v}_B) \\ \rho u(\mathbf{v}-\mathbf{v}_B) + p\mathbf{e}_x \\ \rho v(\mathbf{v}-\mathbf{v}_B) + p\mathbf{e}_y \\ \rho w(\mathbf{v}-\mathbf{v}_B) + p\mathbf{e}_z \\ \rho e(\mathbf{v}-\mathbf{v}_B) + p\mathbf{v} \end{bmatrix} \quad (2)$$

$$\text{and } \mathbf{F^d} = \begin{bmatrix} 0 \\ \tau_{xx}\mathbf{e}_x + \tau_{xy}\mathbf{e}_y + \tau_{xz}\mathbf{e}_z \\ \tau_{yx}\mathbf{e}_x + \tau_{yy}\mathbf{e}_y + \tau_{yz}\mathbf{e}_z \\ \tau_{zx}\mathbf{e}_x + \tau_{zy}\mathbf{e}_y + \tau_{zz}\mathbf{e}_z \\ \psi_x\mathbf{e}_x + \psi_y\mathbf{e}_y + \psi_z\mathbf{e}_z \end{bmatrix}. \quad (3)$$

A detailed description of the diffusive part including the formulation of the symmetrical stress tensor components with Stokes' hypothesis of vanishing pressure viscosity ($\mu_v = \frac{2}{3}\mu$) can be found in [5]. The viscosity is approximated in case of laminar flow by Sutherland's formula as a function of the statical temperature only,

$$\mu(T) = \frac{\sqrt{\kappa}M_\infty}{Re_\infty}\left(\frac{T}{T_\infty}\right)^{\frac{1}{2}}\frac{T_\infty + 100K}{T + 100K}\,. \quad (4)$$

The vector of heat conduction is modeled by Fourier's law ($\mathbf{q} = -k\text{grad}T$) with the heat conductivity k given by a constant Prandtl number Pr

$$k = \frac{\kappa}{\kappa - 1}\frac{\mu}{Pr}\,, \quad Pr = 0.72\,. \quad (5)$$

For turbulent flows, the viscosity μ is replaced by $\mu + \mu_t$ with the turbulent part provided by a turbulence model. In version 113 of the FLOWer code, the algebraic model of Baldwin/Lomax is used. Finally, since air is assumed to behave as a perfect gas, the pressure is calculated by the ideal gas equation of state in terms of pressure, density and internal energy

$$p = (\kappa - 1)\rho\left(e - \tfrac{1}{2}\mathbf{v}^2\right) \quad (6)$$

with κ denoting the ratio of specific heats.

2.2 Underlying Beam Theory

The elastic wing is modeled in ODISA by a Timoshenko-like beam structure with six degrees of freedom for a material cross-section. The centrelines of mass, bending and torsion are generally non-coinciding. By that assumption, besides the coupling via aerodynamics, all degrees of freedom may be coupled with each other mechanically, too. In contrast to the often used Euler-Bernoulli beam theory which couples bending with translation by kinematic constraint involving anomalous dispersion of deformation energy propagation, the Timoshenko approximation with its two more degrees of freedom concerning the shear deformation exhibits no effects of anomalous dispersion and thus describes unsteady deformation in a physically reasonable way.

Extending Hamilton's functional for the wing by terms for the initial conditions δZ_{IC}, boundary conditions δZ_{BC}, the virtual work of airloads

δW^{aero} and energy terms for additional masses (e.g. winglet, engine) δZ_C leads to the variational equation for the complete initial boundary value problem

$$\begin{aligned}\delta I^e(\mathbf{u}_S,\boldsymbol{\varphi}) &= \int_{t_a}^{t_e}\delta\int_0^l l_B d\xi + \delta W^{aero} Dt + \delta Z_C \\ &+ \delta(Z_{IC}+Z_{BC}) \qquad (7)\end{aligned}$$

with the secondary conditions $\delta\mathbf{u}(\xi,t_e)=\mathbf{0}$ and $\delta\boldsymbol{\varphi}(\xi,t_e)=\mathbf{0}$. For the Lagrangian density one obtains

$$\begin{aligned}l_B = \frac{1}{2}(&\rho A\dot{\mathbf{u}}_S\dot{\mathbf{u}}_S + \boldsymbol{\varphi}\boldsymbol{\Theta}_S\boldsymbol{\varphi} - GA\boldsymbol{\gamma}\mathbf{K}\boldsymbol{\gamma} - EAu^2_{B1|1} \\ &- \varphi_{|1}\mathbf{C}_{BTW}\varphi_{|1} + \rho A\mathbf{u}_S\mathbf{g}) \qquad (8)\end{aligned}$$

(S and B are the centers of gravity and bending, respectively). Applying Timoshenko's theory the shear angles are represented as

$$\begin{aligned}\gamma_2 &= u_{S2|1} - \varphi_3 - (\zeta_{SD}\varphi_1)_{|1}\,, \\ \gamma_3 &= u_{S3|1} + \varphi_2 + (\eta_{SD}\varphi_1)_{|1} \qquad (9)\end{aligned}$$

where ζ_{SD} and η_{SD} are the cartesian co–ordinate differences between the center of gravity and the shear center of the cross–section. A detailed description of the remaining terms can be found in [6].

3 Solution Strategy

Within the SOFIA code, the solution schemes for the flow field and the structure are combined in an iterative process through a strong coupling such that the differential equations of both media can be integrated simultaneously i.e. consistent in time. The central time loop works as follows:

ODISA calculates the velocities and the displacements of the structure under the actual aerodynamic loads.

The grid points on the wing's surface (inner boundary of the aerodynamic grid) are moved corresponding to the structure's change of shape. In contrast to the points at the inner boundary the grid points at the outer boundary remain fixed in a rigid-body fixed co-ordinate system. GRIDGEN (GRID GENerator) computes the point distribution such that the topology of the structured grid is preserved.

Finally the flow field and the new airloads are computed for the current time on the numerical grid, which is updated concerning position and state of velocity. This is done by INFLEX solving the Euler equations or in the new version of SOFIA by FLOWer integrating the Navier-Stokes equations. A subiteration level has been implemented which computes the global time step. During repeated calculation an average value of the aerodynamic forces of the current and the preceding time step is used. The iteration is stopped when a certain error bound is reached. Of course, the computer time increases linearly with the (number of) subiteration levels. Numerical experiments have shown that in case of carefully chosen time steps – i.e. all the relevant time scales are resolved properly – just one subiteration is sufficient.

3.1 Numerical Methods

The numerical methods used in SOFIA are desribed here only very shortly. Details are presented in the references.

3.1.1 Flow Solver INFLEX

For the numerical integration of the strong conservation form of the Euler equations an implicit relaxation scheme is used [1]. The unfactored Euler equations are solved by applying a Newton iteration method. Relaxation is performed with a point Gauß-Seidel algorithm. The combination of a Newton method with a point Gauß-Seidel algorithm leads to a robust numerical scheme. Concerning the resolution of pressure and shock waves, a characteristic variable splitting technique is employed. Grid generation is done using elliptical smoothing in every time step.

3.1.2 Flow solver FLOWer

The FLOWer code is being developed in the project MEGAFLOW by different German research organisations under the leadership of DLR/Braunschweig. The numerical discretization of the FLOWer code is based on structured grids. Central differences are used for the spatial discretization. Time integration is performed

by dual-time stepping. Within each pseudo-time step an explicit multi stage Runge-Kutta method is used which is accelerated by techniques of local pseudo-time stepping, enthalpy damping and implicit residual smoothing. The solution procedure is embedded into a sophisticated multigrid algorithm. This flow solver is written in a flexible block structured form enabling treatment of complex aerodynamic configurations with any mesh topology. By coupling a structural solver and an algebraic grid generator [4] the code has been made applicable for aeroelastic analysis.

3.1.3 Structural Solver

To determine the generalized deflections, a second order in time system of ordinary differential equations (ODEs) is derived by applying Hamilton's principle and the method of Ritz/Kantorowitsch [6]. Linear damping is included (Rayleigh-damping). Discretization is done by isoparametric, two–noded elements. A reduced integration scheme avoids shear locking. The set of ODEs is integrated by Newmark's method, where the resulting linear system of equations is solved directly using LU-decomposition. The external forces are assumed to vary linearly during a time-step. Alternatively, the system of ODEs is diagonalized by solving the generalized eigenvalue problem (EVP), and the time integration is done by the evaluation of Duhamel's integral.

4 Results

The focus of this paper is the application of the numerical method SOFIA for the analysis of elastic wings in subsonic flow and the comparison to experimental results of our partners in the Collaborative Research Centre SFB401. The data base will be enlarged to the transonic region by aeroelastic experiments carried out by another partner within the SFB401 in near future. This will make possible a validation of our numerical method in flutter analysis, where the correct modeling of the fluid-structure interaction is essential to capture the strong non-linearities caused by moving shocks and local flow separation. Preliminary results for transonic flow have been published in [8, 9].

Fig. 1 shows the airfoil which has been chosen as reference configuration for all numerical and experimental analyses in the SFB401. Originally defined by the AGARD group in [7] as a three element high lift configuration consisting of slat, main wing and flap (see Fig. 1), we set up a cruise flight configuration by assemblying the parts. Experimental data is provided in [7] only for high lift configuration test cases.

A first set of data for a two-dimensional test case is given in Fig. 3. The calculated pressure coefficient C_p shows a good agreement to the data measured by the Institute of Aerospace Engineering in a low speed wind tunnel at 60m/s flow velocity and zero angle of attack. Since only the main wing is equipped with pressure gauges, the nose and the tail region of the airfoil could not be resolved. The same wing model has been used to analyse the L1T2 high lift configuration defined in [7]. Again, the pressure on the main wing can be predicted very well by the numerics as can be seen in Fig. 4 (M_∞=0.192, α_∞=20.18^o, Re_∞=3.52·10^6). The contour line plot of the Mach number distribution in Fig. 5 shows that the local flow speed on the slat nearly reaches the speed of sound, even though the incoming flow is at M_∞=0.192. Obviously, the use of compressible Navier-Stokes equations is necessary to capture correctly the recirculation zones and flow seperation occuring in this complex flow field.

An elastically very pliable wing model has been built in the Department of Aerospace Structures (Institut für Leichtbau, IfL), particularly to provide experimental data for code validation. Therefore its purpose was not to create as much similarity to a real cruise flight configuration as possible. In contrast to most other wind tunnel models where high stiffnesses i.e. negligible deformation is desired, this wing shows large torsional and bending deformation even under moderate aerodynamic loads at low flow velocity. The specimen is a rectangular wing with a

flap	lag	torsion
$586.39 Nm^2$	$2.177 \cdot 10^4 Nm^2$	$141.329 Nm^2$

Table 1 Average stiffnesses of the wing model

1m semi-span and a chord length of 222mm. A hybrid construction with an aluminum spar and foam defining the aerodynamic shape has been chosen, see Fig. 2. The cross shaped spar admits the realization of a wide stiffness range by varying the length of the notches on the vertical and horizontal parts. The stiffnesses of the model used in the present study are presented in Tab. 1. Since we consider here only steady aeroelasticity, we renounced a detailed representation of the ribs in our numerical model yet and assumed homogeneous spanwise distributions of mass and moments of inertia. The total weight of the fully equipped wing amounts approximately 2.5kg. In the first campaign, no direct shape deformation measurement has been executed. However, high precision deformation information has been made available by a reconstruction method analyzing strain gauges at 16 different spanwise positions. The model has a set of pressure gauges at 50% semi-span. Further details can be found in [11] in these proceedings and in [12].

The standard procedure to determine the wing's steady state aeroelastical equilibrium configuration at a given Mach number and root angle of attack is as follows: At first, the flow field about the undeformed reference configuration is computed. Since for that purpose the fluid solver can be run without coupling to the structural part in "steady" mode, the numerical effort for this first step is relatively low. In the second stage, the unsteady flow field about the deforming wing has to be computed running the code in the "unsteady" coupled mode. Thereby, a fixed support at the wing's root is assumend neglecting the elasticity of flange and support. In order to speed up convergence to steady state, artificial Rayleigh-type structural damping is used. A typical computing time for inviscid flow simulation using 200000 grid points on a vector computer with a performance of 600 MFLOPS takes about two hours. In order to find the zero lift angle of attack of the elastic configuration, normally at least two runs with slightly different root angles of attack are necessary, which do not meet exactly the additional condition of vanishing total lift. However, if the variation of the angle of attack of the two calculations is small enough, e.g. 0.3 degrees, the non-linear fluid-structure system can be assumed to behave linearly within this small range and thus the true zero lift angle of attack can be determined by linear interpolation, i.e. a third run is dispensable.

We have selected four test cases to compare the numerical results computed using the SOFIA code to data measured by the Department of Aerospace Structures:

case	v_∞ $[\frac{m}{s}]$	ρ_∞ $[\frac{kg}{m^3}]$	α_R^{exp} [°]	α_R^{calc} [°]
1	65	1.24	6.93	6.93
2	45	1.24	6.6	6.6
3*)	65	1.21	-1.38	-1.27
4*)	45	1.22	-1.87	-1.7

Table 2 Test case definition (*) cases with vanishing total lift)

Cases 1 and 2 both show a relatively high angle of attack and mainly differ in the wind speed. Cases 3 and 4 are the corresponding cases in which the total lift at the root of the elastic wing vanishes. Since this zero lift angle of attack can be determined very precisely, we have chosen slightly different angles of attack α_R^{calc} than the measured one (α_R^{exp}).

Table 3 gives an overview of the total lift F_2 and and the total torque M_1 at the wing's root. The maximum error in the lift reaches only about 4% (case 2) and about 7% in the torque (case 4).

The complete data set of case 1 is presented in detail in Fig. 6-10. The spanwise distributions of the bending and torsional deformation u_2 and φ_1 respectively are shown in Fig. 6. While the torsional deformation coincides very well over the whole wing span, the bending stiffness at the inner part of the wing seems to be slightly overestimated in the calculation. In Fig. 7 the pressure coefficient C_P at 50% of the semi-span is dis-

	F_2 [N]		M_1 [Nm]	
case	exp	calc	exp	calc
1	486.9	498.4	9.58	9.57
2	204.3	212.7	4.04	3.71
3*)	<1	<1	-6.52	-7.02
4*)	<1	<1	-3.17	-3.41

Table 3 Total forces and moments at the wing's root (*) denotes cases with vanishing total lift)

cussed. A very good agreement to the measured data can be seen. Fig. 8 gives information about the spanwise distribution of lift and moment coefficient C_L and C_M respectively. In this figure the distributions for the rigid case have been added to demonstrate the big difference for this very flexible wing. Fig. 9 shows the time history of the translation and the rotation of the wing tip during the unsteady simulation. Due to high artificial Rayleigh-type damping chosen here the translation reaches its asymptotically steady state relatively fast, while it takes a little more time for the rotation to converge. Finally, Fig. 10 shows a qualitative comparison between experiment and calculation. Though the point of view of the twice-exposed photograph in the upper part of this figure showing the wing in the wind tunnel is not exactly the same as in the computational result below, this figure gives quite a good impression about the flexibility of the wing.

Concerning case 2 we refer to the work of our partners of IfL published in these proceedings [11], too.

The angle of attack for which the total lift of the elastic wing vanishes represents another parameter suitable for code validation. Fig. 11 shows the zero lift angle of attack versus the wind speed. As can be seen in this figure the agreement between the computational and experimental data becomes very good with higher wind speeds. The reason for that can be found in Table 4. Herein, the total lift for the rigid wing with a root angle of attack corresponding to the zero lift case of the elastic wing is given. Since the total lift reaches only 3.8N for flow velocity 35m/s, the deformation of the wing remains very small which is synonymous with a relative great error in both, experiment and in calculation. On the upper limit at a wind speed of 85m/s, we have a load of 125.5N in the rigid case leading to considerable deformation and thus a smaller error percentage.

Fig. 12-15 finally show the spanwise deformation distribution and the pressure coefficient at 50% semi span for cases 3 and 4. Though the relative differences between measured data and the calculation using the SOFIA code are greater than in the cases discussed before, the results are quite satisfying.

v_∞ [m/s]	35	45	55	65	75	85
α_{W0}^{calc} [°]	-1.8	-1.7	-1.5	-1.27	-1.0	-0.64
F_{W2} [N]	3.8	9.8	22.3	42.7	75.1	125.5

Table 4 Total lift vs. wind speed for the rigid wing with root angle of attack yielding zero lift in the elastic case.

5 Conclusions and outlook

In this paper the SOFIA code for direct numerical simulation of fluid/structure interaction has been presented. Using the domain decomposition technique the non-stationary flow is modeled either by the Euler equations or by the Navier-Stokes equations, and the wing structure is modeled by a generalized quasi one-dimensional theory based on Timoshenko's beam theory.

Numerical results are shown for rigid and elastic reference configurations of the Collaborative Research Centre SFB401 "Modulation of Flow and Fluid-Structure Interaction at Airplane Wings" for low Mach number cases. Detailed comparison of calculation and measurement is presented for the aeroelastic equilibrium position of a higly flexible rectangular wing model. Besides two test cases with high angles of attack at the wing's root, the dependence of the zero lift angle of attack on the wind speed is discussed. Numerical and experimental results for the spanwise deformation and the pressure distribution agree very well. However, the difference in the zero lift angle of attack between experiment and

computation rises up to approximately 0.2 degrees when flow velocity decreases because of decreasing aerodynamic load and very small deformation and therefore greater relative errors in experiment and in simulation as well.

Future work will include dynamic anlysis of the elastic wing requiring a detailed modeling of the wing's mass and inertia distribution concernig ribs, measuring equipment etc. Furthermore, we will concentrate on dynamic stability analysis in the transonic regime to provide data for design of corresponding experiments.

6 Acknowledgements

This work has been supported by the Deutsche Forschungsgemeinschaft (DFG) in the Collaborative Research Centre SFB 401 "Modulation of Flow and Fluid-Structure Interaction at Airplane Wings" at the RWTH Aachen University of Technology. The experiments concerning the reference configurations of the SFB were accomplished by the Institute of Aerospace Engineering and the Department of Aerospace Structures of RWTH. Computations were performed using the NEC-facilities of the High-Performance Computing-Centre Stuttgart (HLRS). We would like to thank Dr. A. Brenneis and Dr. A. Eberle from DASA for providing the computer code INFLEX as well as Dr. R. Heinrich from the German Aerospace Research Establishment (DLR/Braunschweig) and all partners within the project MEGAFLOW developing the FLOWer code.

References

[1] Brenneis A., Eberle A. (1992) Evaluation of an Implicit Euler Code Against Two and Three-Dimensional Standard Configurations, AGARD CP-507: Transonic Unsteady Aerodynamics and Aeroelasticity, Paper No. 10

[2] Kroll N., Radespiel R., Rossow C.-C. (1994) Accurate and Efficient Flow Solvers for 3D Applications on Structured Meshes, Lecture Series 1994-05 of the von Karman Institute of Fluid Dynamics

[3] Jameson A. J. (1991) Time Dependent Calculation using multigrid, with Applications to Unsteady Flows past Airfoils and Wings, AIAA paper 91-1596

[4] Werle M. (1997) Gittergenerierung für die Strömungssimulation von elastischen Auftriebskörpern, diploma thesis, RWTH Aachen

[5] Heinrich R., Pahlke K., Bleecke H. (1996) A Three Dimensional Dual-Time Stepping Method for the Solution of the Unsteady Navier-Stokes Equations, Proc. RAS 'Unsteady Aerodynamics' Conference in London, pp. 5.1-5.12

[6] Nellessen D. (1995) Schallnahe Strömungen um elastische Tragflügel, Fortschrittsberichte VDI Reihe 7: Strömungstechnik, Nr. 302

[7] Moir I.R.M. (1994) Measurements on a Two-Dimensional Aerofoil with High-Lift Devices, AGARD AR-303, Test Case A2

[8] Britten G., Ballmann J. (1999) About the Uniqueness of Aeroelastic Solutions of Elastic Wings in Transonic Flow, NNFM 72, pp. 77-84

[9] Britten, G. Ballmann, J. (1999), Navier-Stokes-Based Direct Numerical Simulation, CEAS Conference on Aeroelasticity and Structural Dynamics, Paper No. A4/1

[10] Özger E., Jacob D. (1999) Wirbelbeeinflussung an Tragflügeln, SFB401 – Arbeits- und Ergebnisbericht 1999, RWTH Aachen, pp. 7-47

[11] Kämpchen M., Jung W., Dafnis A., Reimerdes H.-G. (2000) Design and Qualification Concepts for Flexible Wind Tunnel Models, Proc. ICAS 2000, Paper No. ICA0466

[12] Kämpchen M., Jung W., Dafnis A., Reimerdes H.-G. (1999) Entwicklung elastischer Flügelmodelle und experimentelle Untersuchungen im Windkanal sowie Konzepte und Modellierung der Tragstruktur elastischer Flügel, SFB401 – Arbeits- und Ergebnisbericht 1999, RWTH Aachen, pp. 343-386

[13] Ballmann J. (1999) Strömungsbeeinflussung und Strömungs-Struktur-Wechselwirkung an Tragflügeln – Erste Ergebnisse des SFB401 der RWTH Aachen, DGLR-JT99-189

7 Figures

Fig. 1 Cruise flight reference configuration (based on the 3 element high-lift configuration BAC 3/11/RES/30/21 [7])

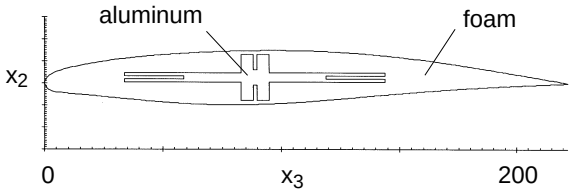

Fig. 2 Cross-section of the aeroelastic wing model of the Institute of Lightweight Structures.

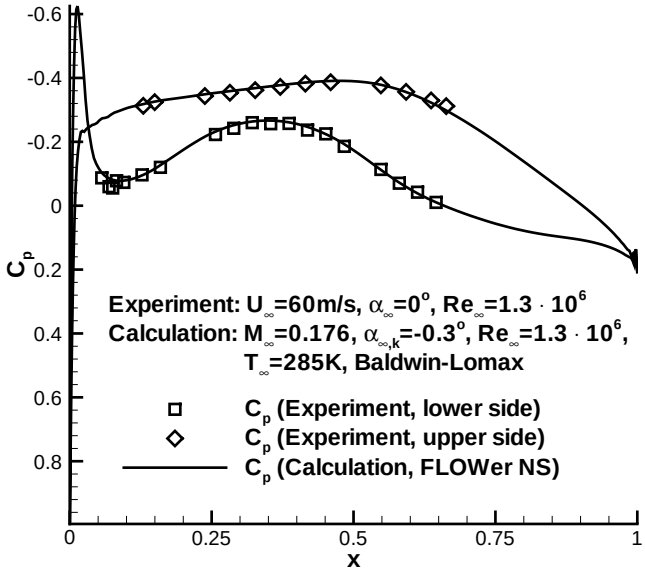

Fig. 3 Comparison of numerical and experimental results for the SFB reference airfoil

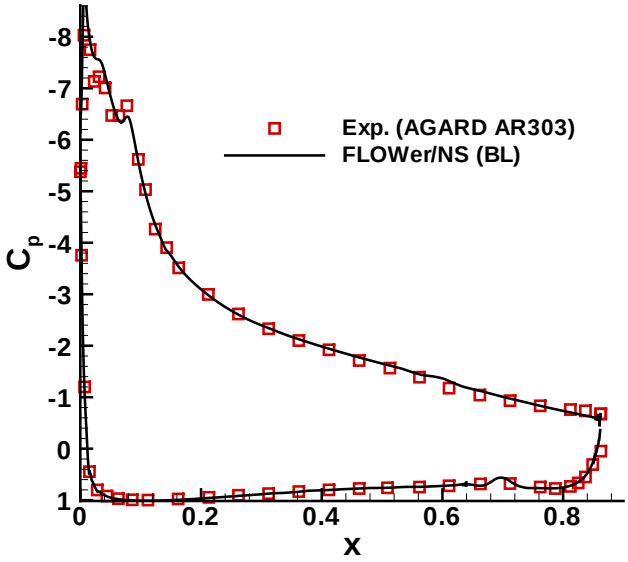

Fig. 4 Comparison of numerical and experimental results of [7] for the high lift reference configuration (M_∞=0.192, α_∞=20.18°, Re_∞=3.52·10^6)

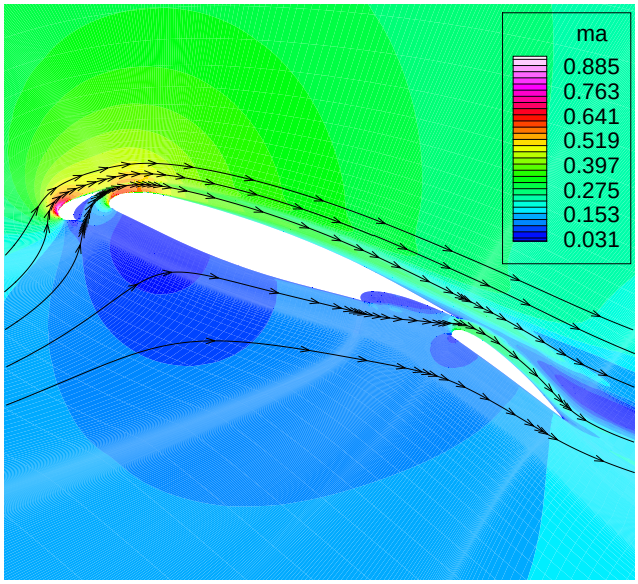

Fig. 5 Contour lines of the Mach number for the high lift confiugration (M_∞=0.192, α_∞=20.18°, Re_∞=3.52·10^6)

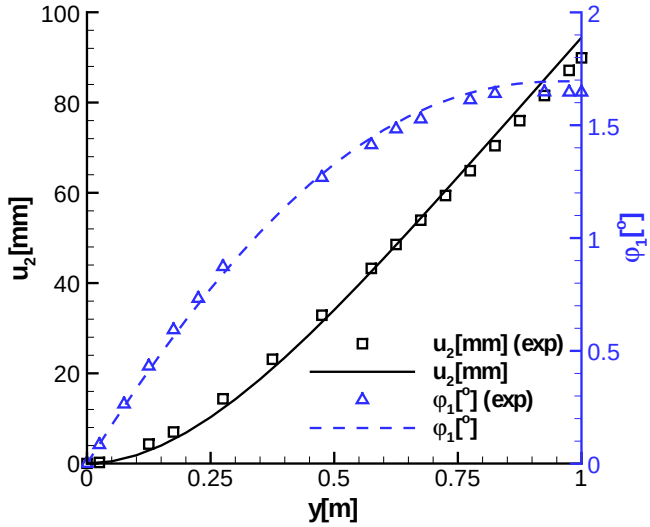

Fig. 6 Comparison of measured and calculated spanwise bending and torsional deformation (case 1)

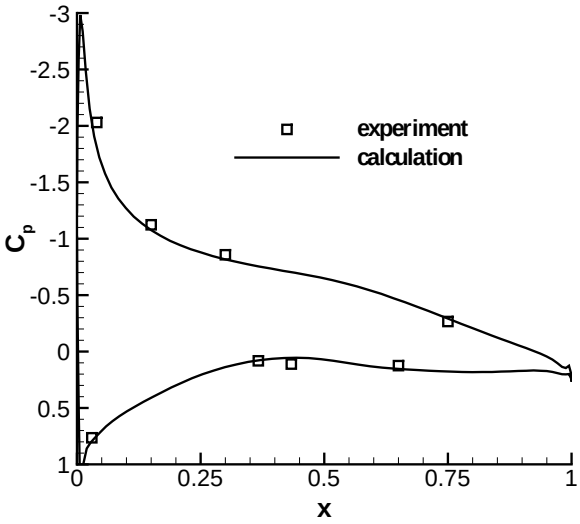

Fig. 7 Comparison of measured and calculated pressure coefficient in a cross-section at 50% semi-span (case 1)

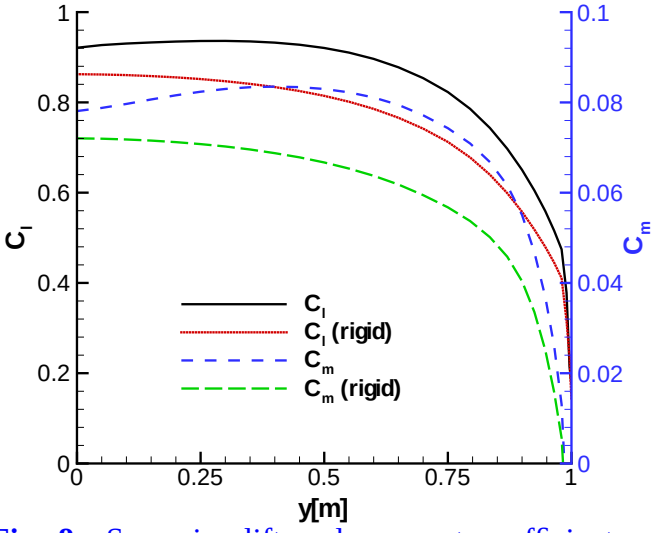

Fig. 8 Spanwise lift and moment coefficient (case 1)

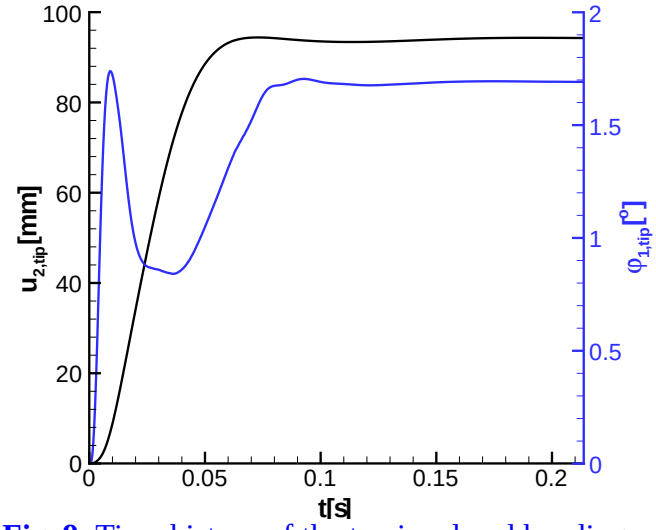

Fig. 9 Time history of the torsional and bending deformation at the wing's tip (case 1)

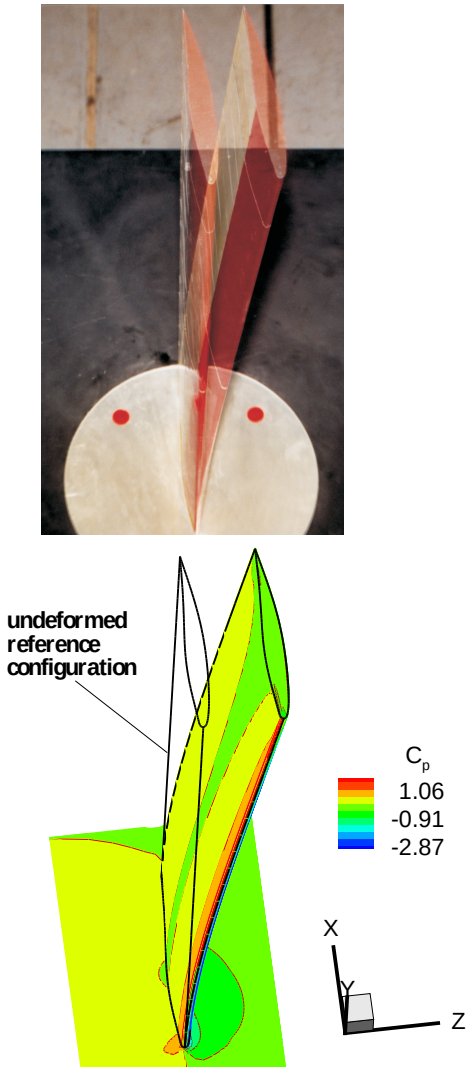

Fig. 10 Rectangular wing in aeroelastical equilibrium configuration (case 1)

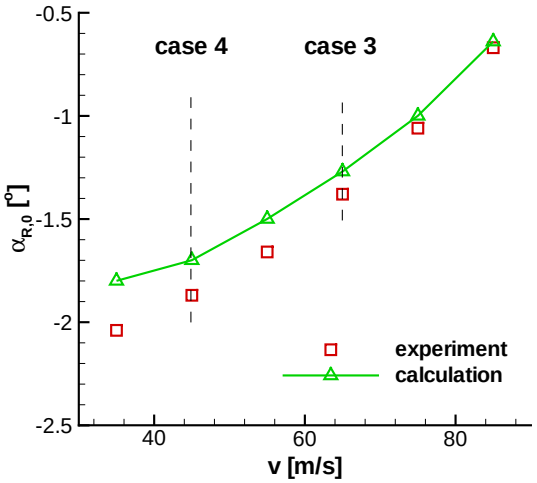

Fig. 11 Comparison of measured and calculated zero-lift angles of attack at the wing's root.

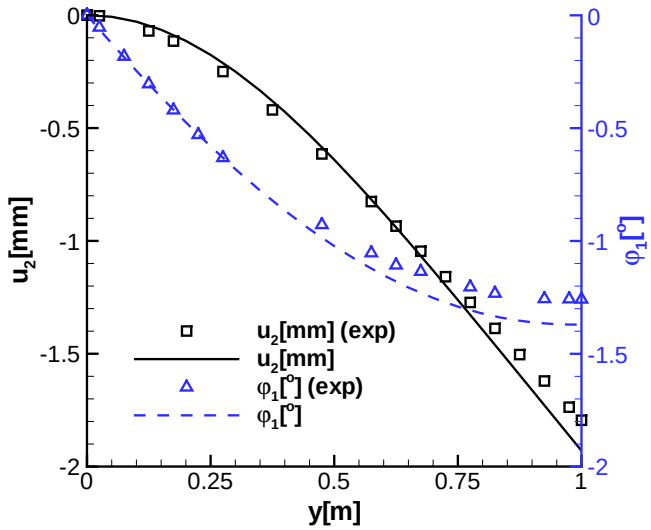

Fig. 12 Comparison of measured and calculated spanwise bending and torsional deformation (case 3)

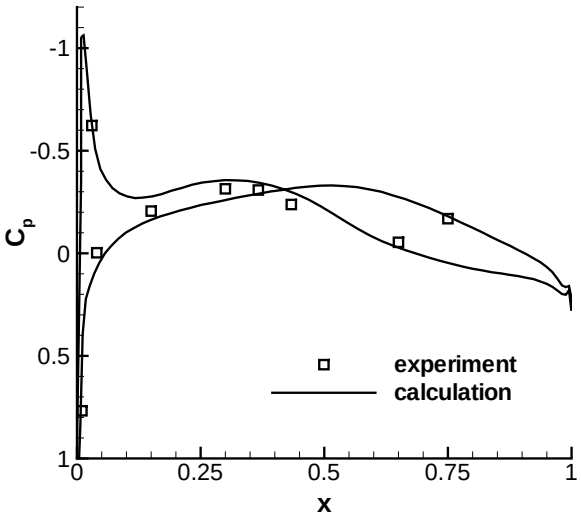

Fig. 13 Comparison of measured and calculated pressure coefficient in a cross-section at mid span (case 3)

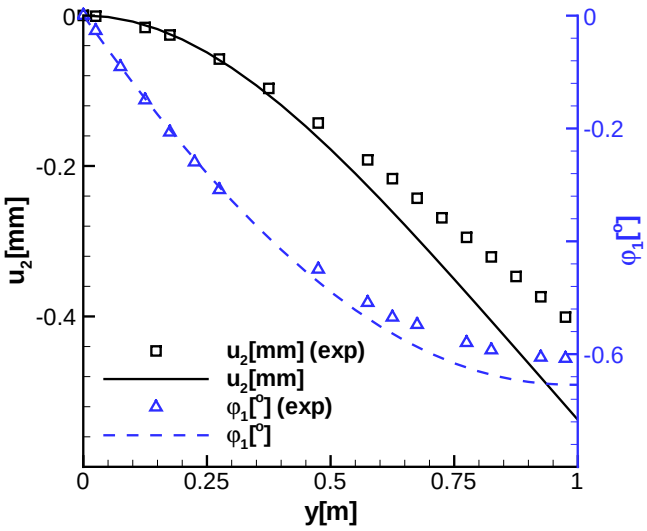

Fig. 14 Comparison of measured and calculated spanwise bending and torsional deformation (case 4)

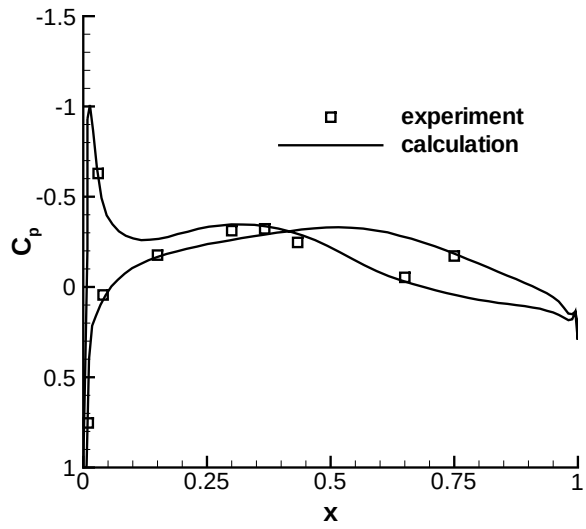

Fig. 15 Comparison of measured and calculated pressure coefficient in a cross-section at mid span (case 4)